Materials Science & Engineering A 824 (2021) 141818

Contents lists available at ScienceDirect

Materials Science & Engineering A

journal homepage: www.elsevier.com/locate/msea

Prolonged high-temperature exposure: Tailoring nanocrystalline Cu–Ta alloys against grain growth

B.C. Hornbuckle [a,*], K. Solanki [b], K.A. Darling [a]

[a] Army Research Laboratory, Aberdeen Proving Ground, MD, 21005, USA
[b] School for Engineering of Matter, Transport, and Energy, Arizona State University, Tempe, AZ, 85281, USA

ARTICLE INFO

Keywords:
Thermal stability
Nanocrystalline
Scanning transmission electron microscopy
High temperature

ABSTRACT

In this work, various alloy compositions of immiscible copper-tantalum (Cu–Ta) are systematically studied to understand the interplay between cluster stability, precipitation hardening, and the overall stability of the matrix's average grain size. An alloy composition of Cu-3at.%Ta is found to exhibit dramatic improvements relative to other neighboring Ta contents (both higher and lower) only after exposures of more than 300 h at 800 °C. An extremely low steady-state growth rate, i.e., 3.1 nm per 100 h exposure, speaks to the extreme kinetics which allow this composition to retain its high mechanical strength. The key attribute responsible for the NC Cu-3at.%Ta alloy exhibiting such behavior is a high cluster density tailored through the Ta solute content to achieve the best combination of stability without sacrificing strength by limiting Orowan coarsening of the clusters compared to other Ta concentrations. In general, the growth kinetics of this Cu-3at.%Ta alloy are so sluggish that it places it among the most thermally resistant alloys ever produced. The work demonstrates that, if designed properly, bulk nanocrystalline alloys can withstand the prolonged high-temperature exposure required for high-temperature applications, while grain growth is stagnated or halted.

1. Introduction

The major technological challenge for advanced alloy development has always centered on designing an alloy to resist microstructural changes. This is most typified for alloys designed for the nuclear and aerospace industries, where millions of dollars in fundamental and applied research have been spent in designing heat resistant alloys to allow for successful long-term operation (thousands of hours) [1,2]. Here, alloys are expected to operate continuously at homologous temperatures above 70% of their melting point with minimal change in their microstructure and mechanical properties, such as under creep/dwell-fatigue conditions [3]. This is a regime in which bulk nanocrystalline (NC) metals, despite their advantages over conventional alloys, have not been expected to access much less excel. This is because the extreme physical properties that NC metals possess are linked to maintaining a small average grain size [4]. These instabilities have been summarized in the following review articles with a focus on thermal stability and methods to minimize and/or restrict grain growth [5–7]. In addition to thermal instabilities in grain size, mechanical and thermo-mechanical stress have lead to rapid instabilities in grain structure [8–11]. Furthermore, multiple studies have attempted to identify and quantify the underlying reason leading to the grain growth in NC materials due to temperature including grain boundary diffusion, limited solute at grain boundaries, lower activiation energy for grain growth than lattice diffusion, and grain boundary sliding/rotation [12–16].

To further elaborate on these issues, instability in NC metals has been extensively observed under various annealing experiments in literature [17–22]. For example, NC Pd shows abnormal grain growth even at room temperature conditions [17]. Grain growth of several orders in magnitude was observed up to temperatures of 773 K ($0.56T_m$) in NC Cu films by Simoes et al. [18]. Moreover, grain boundary migration at elevated temperatures resulted in similar abnormal grain coarsening in multiple studies on NC Ni [20,21]. In addition to thermally-assisted grain coarsening, NC metals and alloys also tend to show mechanically-assisted, or both thermo-mechanical driven coarsening. Mechanically-assisted grain growth has been reported either under monotonic loading, or cyclic loading of different NC materials [23–28]. For instance, Padilla et al. reported that cyclic loading of NC Ni–Mn resulted in micron-sized grains near the vicinity of the crack tip. Gianola et al. [28] studied the room temperature stress-assisted grain growth in NC Al films using micromechanical experiments and reported an almost

* Corresponding author.
E-mail address: billy.c.hornbuckle.civ@mail.mil (B.C. Hornbuckle).

https://doi.org/10.1016/j.msea.2021.141818
Received 25 March 2021; Received in revised form 23 July 2021; Accepted 26 July 2021
Available online 27 July 2021
0921-5093/Published by Elsevier B.V.

four-fold increase in the initial grain size. Thermo-mechanical induced microstructure instability has been previously reported under creep conditions at room temperature as well as high temperatures [29–33]. For example, grain boundary diffusion based mechanism was observed under tensile creep at around room temperature ($0.22T_m$ – $0.24T_m$) in pure NC Cu [31]. Similarly, almost a three-fold increase in grain size was observed during room temperature creep of NC Ni by Li et al. [33]. Despite the potential advantages of refining the microstructure in pure metals and alloys, microstructural instability has often rendered making bulk NC parts (where the overall grain size distribution does not exceed about 100 nm) a big challenge. As such, the applicability of NC materials for structural applications is yet to be fully evaluated in literature.

Recently, though, it was reported that under creep conditions a kinetically pinned (Zener pinning [34]) NC-Cu-10Ta alloy was stable enough to resist deformation by exhibiting a 6–8 orders of magnitude lower steady-state creep rate as compared to pure NC-Cu [35,36]. This finding substantiates bulk NC metals as viable options for long-term elevated temperature applications (such as turbine casing/blades, heat exchanger, etc.); however, times approaching 1,000 to 10,000 h or greater (especially for heat exchanger and turbine blade applications) are needed to validate for time scales of practical use. This leads to the question. If the exposure time is 1–2 orders of magnitude longer in real applications, is the perceived stability for NC alloys highlighted in literature after a few hundred hours or less, a relevant comparison to commercially available alloys (such as Fe-based or Ni-base alloys) successfully used for thousands of hours [35–37]? The long-term stability is critical from the practical application viewpoint. Since the ability for diffusion to occur increases dramatically with respect to temperature, this is especially true in nanocrystalline materials with their elevated number of grain boundaries acting as fast diffusion pathways. Such an increase in atoms ability to easily diffuse will introduce instability leading to a loss in strength as well as premature failure. Therefore understanding prolonged thermal behavior is critical. Further, while varying Ta content, the manuscript also highlights an important point that it is critical to study a long exposure time since some of the kinetic mechanisms may be very slow in such constraint systems (constraints are referred to having extremely high defect densities that can slow down some kinetic process) and the true nature (behavior) is only attainable through such exposure. Hence, such demonstrations and tailoring of compositions are the logical steps if bulk NC metals are to be seriously considered viable candidates for advanced high-temperature applications, such as heat exchangers for nuclear applications and some turbine blade applications.

2. Experimental details

Towards this, a series of immiscible Cu–Ta alloys with Ta contents of 0.25, 1, 3, 5, and 10 (at.%) were mechanically alloyed through ball milling. The milling process was performed in a dual-vial SPEX 8000M shaker mill. Elemental Cu and Ta powders (~325 mesh, 99.9% purity) were loaded into hardened steel vials along with 440C stainless steel ball bearings in a glovebox with an Argon (Ar) environment ($\geq$1 ppm of O_2 and $\geq$1 ppm of H_2O) to minimize oxidization. All compositions were generated using a ball to powder ratio of 10:1 with a combined 10 g of powder initially loaded into the vials. The milling process was carried out for 4 h at cryogenic temperatures (−196 °C) by flowing liquid Nitrogen around the vials during the entire milling process (The vials were held in place by nylon sleeves that were machined to allow for a continuous inward and outward flow of liquid nitrogen).

Once milled, 3 mm diameter compacts of each composition were made by uniaxially pressing the as-milled powder at 3 GPa in tungsten carbide dies. All 1-h annealing treatments were placed in a quartz tube within a tube furnace. During these heat treatments, all compacts were wrapped in Ta foil and a continuous flow of Ar was passed over them to minimize oxidation. For the 100 and 1,000 h heat treatment, the compacts were again wrapped in Ta foil then encapsulated in a quartz tube backfilled with Ar to minimize oxidation and Ar consumption over such long periods.

Vickers micro-hardness was performed using a Wilson Hardness Tukon 1202 tester to measure the hardness for all compacts from the as-milled to the 1,000 h heat-treated condition. To do such measurements, the compacts were taken through a grinding and polishing procedure that ended with at least a 1-μm diamond suspension step. The individual indents were generated using a 100 g force and held for 10 s. Ten indents were performed for each data point reported in this manuscript, and the indents were measured randomly from all over the entire surface of the compact to ensure a true sampling was taken. Also, the resulting hardness values were converted to yield strength using an appropriate conversion factor (by multiplying with ~3.27) [38]. Further details of the polishing technique along with other information about indentation experiments can be found in Refs. [39,40].

Transmission electron microscope (TEM) and atom probe tomography (APT) specimens were lifted out directly from the 3 mm diameter compacts of their respective composition and annealing conditions. An FEI Nova600i Nanolab dual-beam focused ion beam (FIB)/scanning electron microscope (SEM) was utilized to generate both the TEM and APT samples, respectfully. The TEM analysis was conducted using a JEOL 2100F (scanning) TEM ([S]TEM) microscope operated at 200 kV. Atom probe tomography was performed using a Cameca LEAP 5000 XR system operated at 50 K with a laser energy of 50 pJ, auto pulse rate control enabled with a minimum mass spectrum range of 300 Da, and target evaporation rate of 0.5%. The analysis was performed using IVAS 3.8.4 software. The envelop method was utilized for the cluster analysis with a maximum separation distance of 0.75 nm (d_{max}); a group of Ta ions with more than 15 ions (N_{min}) was identified as a cluster. Finally, an envelop distance (L) of 0.38 nm was designated for all Cu ions to be included within the cluster, while any ion at a distance greater than 0.38 nm ($d_{erosion}$) from any other ion defining the cluster's perimeter was excluded.

3. Results and discussion

Though systems such as NC Cu–Ta have shown promise for high-temperature applications such as turbine blades, no critical experiments focused on designing or tailoring chemical compositions for prolonged high-temperature exposure have been undertaken [39–42]. To this point, can a nanocrystalline system that depends on the kinetic pinning (Zener pinning) of grain boundaries such as Cu–Ta be forced, by tailoring composition, to exist in a deep metastable state?

Specifically, under equilibrium conditions, the Cu–Ta system is immiscible having zero mutual solubility. High-energy ball milling pushes the Cu–Ta system to a far from equilibrium, highly defective state in the form of a supersaturated solid solution, where the grain size approaches the limits of nano-crystallinity. It is known that cryogenic ball milling can affectively disperse up to ~3–4 at.% Ta within the Cu lattice. Of this 3-4 at.%, some fraction exists as a substitutional solid solution of Ta in Cu, and the remainder Ta–Cu based coherent clusters having an average diameter of 2–3 nm (these clusters reside within the Cu lattice and along grain boundaries). With that in mind, isothermal exposure of the ball-milled materials to moderately high temperatures (i.e. 100-600 °C) for a few hours causes the highly defective microstructure to evolve through grain growth, decomposition, and restructuring [39]. With regard to this decomposition process, the former solid solution between Ta and Cu breaks down to (1) form more coherent clusters, increasing both the hardness and Zener pinning force. This process can be considered a pre-treatment or initialization of the microstructure. Initialization speaks to the evolution of the spatial arrangements and microstructural length scales that are generated (i.e., the average Cu grain size and the average Ta-based clusters diameter and density), during this initial thermal exposure. This initialized microstructure has been found to be fixed and resistant to further change during short-term exposures (i.e., <100 h). The degree to which the microstructure is tuned for long-term

stability at high homologous temperatures can be modified by adjusting the Ta composition. That is, while a wide compositional range has been shown whereby the microstructure can be stabilized under these shorter times and moderate temperatures, differences in stability induced by changing the composition of Ta were found to be marginal [35–37,39–41,43]. However, for much longer-term (i.e., >100 h) and higher temperatures (i.e., >70% T_M), the resultant initialized microstructure and hence composition plays a more critical role in determining prolonged stability. This fact primarily relates to the extremely slow diffusion of Ta in the Cu lattice, and the degree to which it controls phase separation even approaching the melting point of Cu [44]. For instance, if the bulk composition is above 3–4 at.% the additional Ta becomes distributed as larger incoherent Ta particles ranging in size (10–30 nm) having the same spatial distribution as the smaller 2–3 nm clusters. This is due to the inability of high-energy cryogenic ball milling to force a higher metastable solid solution between Cu and Ta. However, (2) a higher solute concentration results in a higher driving force for Ostwald ripening. That is an increase in un-dissolved Ta-based particles (coherent and incoherent) may simply grow easier without the need for nucleation. This consequently limits the number density of nanoscaled Ta particles efficient at pinning grain boundaries resulting in the loss of strength and grain growth. However, the extremely sluggish diffusion of Ta thereby provides a method to kinetically limit cluster nucleation and coarsening by controlling the amount of solute present during thermal decomposition. For example, assuming homogenous nucleation (i.e., as in spinodal decomposition [34,44]) the diffusion length between clusters increases with lower and lower dissolved Ta solute content. As the cluster separation increases, so does their resistance to coarsening. However, (3) the increase in cluster stability associated with the lower solute content (i.e. longer diffusion path) comes at the cost of lowering their number density. Therefore, there should exist a maximum between these two competing effects namely (2 and 3) that is too high of a Ta concentration results in rapid cluster coarsening, and too low of Ta concentration yields an ineffective cluster density. Both of these effects reduce the Zener pinning force (which inherently governs the Cu grain size stability and retained strength). Finally, Ostwald ripening of clusters is a time and temperature-controlled process. This is especially true in the case of immiscible Cu–Ta alloys where substitutional diffusion is extremely frustrated, and excess thermal energy is required for Ta's diffusion [44]. Consequently, these evolutionary processes can be seen with the change in yield stress between the as-milled and conditions isothermal annealed for 1 h from 200 °C to 1050 °C for the various alloy compositions as seen in Fig. 1. The plot indicates that generally lower concentrations of solute tend to be more stable with respect to retaining mechanical response at moderate temperatures with the exception being the Cu-0.25Ta composition. As the temperature continues to increase toward the melting point (1000 °C, i.e., > 0.9 T_M), the microstructural evolution at these higher temperatures provides some insight into longer exposure times. This is best seen whereby 3% Ta exhibits greater retention of strength due to the balancing of the two aforementioned effects as compared to the neighboring composition both higher and lower.

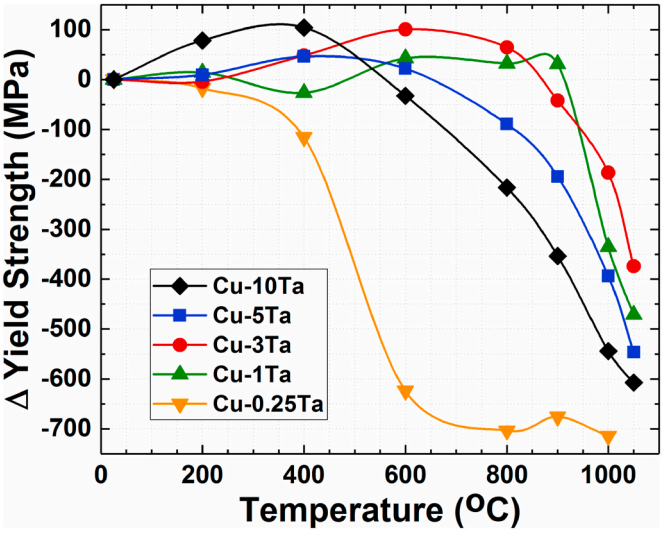

Fig. 1. Change in yield strength between each compositions' as-milled yield strength and after 1 h of isothermal annealing at temperatures from 200 °C to 1050 °C.

Reaching higher temperatures and/or prolonged times is therefore the only way to delineate differences in instability as a function of Ta content at low to moderately high temperatures (400–800 °C, i.e., < 0.8 T_M). It should be mentioned that these aspects pertain only to the effectiveness of kinetically pinning the Cu grain boundaries through Zener pinning. Keep in mind, these same grains are trying to reach equilibrium through the curvature-driven force/pressure of grain growth, the kinetics of which are controlled by Cu self-diffusion via grain boundary mobility.

To substantiate the role Ta clusters play in retaining the initialized microstructure, atom probe cluster analysis has been performed for the temperature range (i.e., 24-400 °C) over which thermal decomposition occurs for Cu-10at.% Ta. It can be seen from new Table 1 that a maximum cluster density of 31.7 x 10^{23} m^{-3} centers around 200 °C (which is over 2 times higher than for all other temperatures listed in the Table). Additionally, it can be seen that the average cluster size (diameter in nm) increases from 3.56 ± 1.8 nm at 100 °C to approximately 5 ± 1.8 nm at 400 °C for the Cu–10Ta alloy. As the clusters precipitate and evolve (Table 1), Cu–10Ta shows a peak in strength over the same temperature range (24–400 °C) when isothermally annealed for 1 h, Fig. 1. Interestingly when understanding the cluster evolution process and applying it to other compositions in Fig. 1, it becomes apparent that the peak strength for 1, 3, and 5 Ta is pushed to and retained at higher temperatures when compared to Cu–10Ta. This increase in cluster density is a measure of and the degree to which thermal decomposition of the former solid solution between Ta and Cu has occurred, while also being dependent on the initial solute content. Case in point, previous work has shown that Cu-1at.%Ta has a 37% decrease in the number density of Ta cluster relative to Cu-10at.%Ta [41]. Moreover, despite the order of magnitude change in the Ta content, the cluster's average size was determined to be essentially identical between the two alloys. As seen in Fig. 1, the peak strengthening in Cu–10Ta is more substantial but decays much more rapidly with increasing temperature due to the evolutionary difference in their cluster density. In other words, under short exposure to moderate temperature, the average cluster size is independent of the bulk Ta content with only the number density increasing between the two alloys [41]. Thus to establish a true understanding of the Ta clusters coarsening kinetics and the effect on the overall microstructural stability, much longer times and/or high-temperature exposures (i.e., those greater than 10 h and 600 °C) are required. Since the grain size for all alloys is constantly evolving to a larger average size with increasing temperature, its contribution can only cause a reduction in the overall trends observed; thus any positive increases in the yield stress are directly related to thermal decomposition and cluster formation as provided in Table 1. Further, there is a possibility of dislocation partial punching out of the grain boundary

Table 1
Cluster diameter and density determined from the atom probe of Cu–10Ta after isothermal annealing for 1 h at 100, 200, 300, and 400 °C.

Cu–10Ta (at.%)	Cluster Diameter (nm)	Cluster Density (per m^3)
100 °C	3.56 ± 1.8	13.9E+23
200 °C	4.12 ± 1.7	31.7E+23
300 °C	5.18 ± 2.3	14.4E+23
400 °C	5.0 ± 1.8	14.2E+23

(relaxation process) also playing a role in observed increases in the yield stress. However, generally these temperatures are well above those associated with a recrystallization and relaxation in NC Cu, which occurs approximately between 100 and 150 °C. Therefore, the peak strength is better explained by the higher temperature cluster precipitation and hardening effect (200–600 °C) as described earlier and shown in Fig. 1.

To gain further insight and show the true compositional dependence of long-term elevated temperature effects, Fig. 2 provides isothermal annealing plots showing the change in strength relative to each alloy's respective peak strength at various fractions of T_M (1357.6 K) for up to 1,000 h of exposure (additional plots showing the raw strength are provided in Appendix Fig. A1). Additionally, Fig. 2 has been replotted with a log scale, Fig. A2, to highlight the changes occurring at the shorter time scales. The obvious trend after annealing when observing the raw data in supplemental is a staggering increase in yield strength with Ta concentration with 10% being the greatest. This is especially true for annealing at 400 °C and 600 °C. When viewing changes in yield strength for Fig. 2A (400 °C curve), the highest and lowest solute amounts, 0.25% and 10% Ta, interestingly display negative slopes after 100 h of annealing, while the middle solute amounts of 1, 3, and 5% Ta show positive slopes. This speaks to the microstructures for the highest and lowest solute amounts undergoing a detrimental evolutionary effect with extended time at a temperature from their initialized state. While the middle compositions appear to behave in a beneficial way with 3% having the most pronounced benefit. This is again related to the intermediate composition of Cu–Ta having undergone a precipitation strengthening process that has been retained at much longer times as compared to Fig. 1. The Cu–3Ta alloy shows the greatest increases in peak strength of the intermediate compositions, while simultaneously retaining this strength better than Cu–5Ta alloy.

From the change in strength plot, Fig. 2B (600 °C curve), it is observed that curves for 10, 5, and 1% all show a noticeable decrease from their peak yield stress (the highest yield stress attained), while 3% shows a negligible decrease. That is, there is only a 2% difference in the strength for the 3% Ta composition after exposure for 1,000 h at 65% T_M. Further, the critical observation is that alloys with various compositions are staggered with lower Ta solute concentrations having a greater ability to retain strength relative to those with higher solute contents. For instance, the 1% Ta alloy retained a 900 MPa yield strength after 1,000 h of exposure to 65% T_M. However, despite measuring differences in their response, the grain sizes for 1, 3, and 5 at. % Ta show little to no discernible differences post-annealing. Specifically, the STEM bright-field images, Fig. 3 A-C, confirm negligible changes between 3 and 5% Ta alloys, while the 1% exhibits minimal grain growth. This is consistent with earlier work by the authors on this family of alloys, where shorter time studies revealed little difference with regard to microstructural evolution and performance of the alloys [39,40,45–47]. However, the 800 °C curves, Fig. 2C and 2D, clearly delineate a difference and show the compositional tailoring with regard to long-term stability. By going to 800 °C, all compositions now display a negative slope with extended time with the magnitude and strength loss being ~3 to 5 times more for the other alloy compositions compared to 3% (i.e. Fig. 2C). This equates to a 500–700 MPa decrease in yield strength when exposed to 800 °C for an extended time for the other compositions. That said, the critical observation that alloys with lower Ta solute concentration having a greater ability to retain strength relative to those with higher solute contents persist with 10, 5, and 1 Ta with 3% being an outlier. By considering Fig. 2B–D, it validates 3% being the most resistant to change in its strength over this time, temperature, and Ta composition range. Interestingly, the raw yield stresses (Fig. 2D) for the 3, 5, and 10% Ta alloys are roughly the same from 1 to 100 h of aging, but after approximately ~ 2 weeks, the strength of 1, 5, and 10% continues to drop at a more increased rate than the 3% Ta alloy. In other words, there exists a transition range in time, where the 3% composition

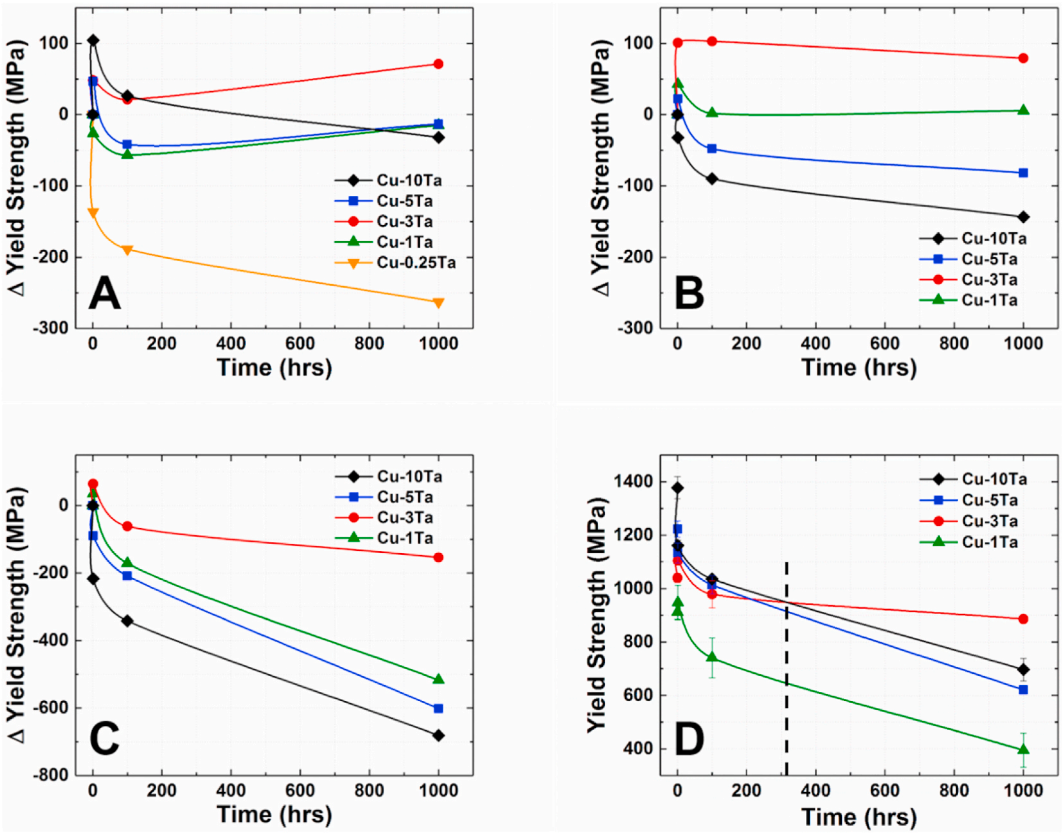

Fig. 2. Change in yield strength relative to each compositions' as-milled yield strength after 1,000 h of isothermal annealing at (a) 400 °C (50% T_M), (b) 600 °C (65% T_M), and (c) 800 °C (80% T_M) respectively. (d) Yield strength curves for the various compositions aged at 800 °C out to 1,000 h.

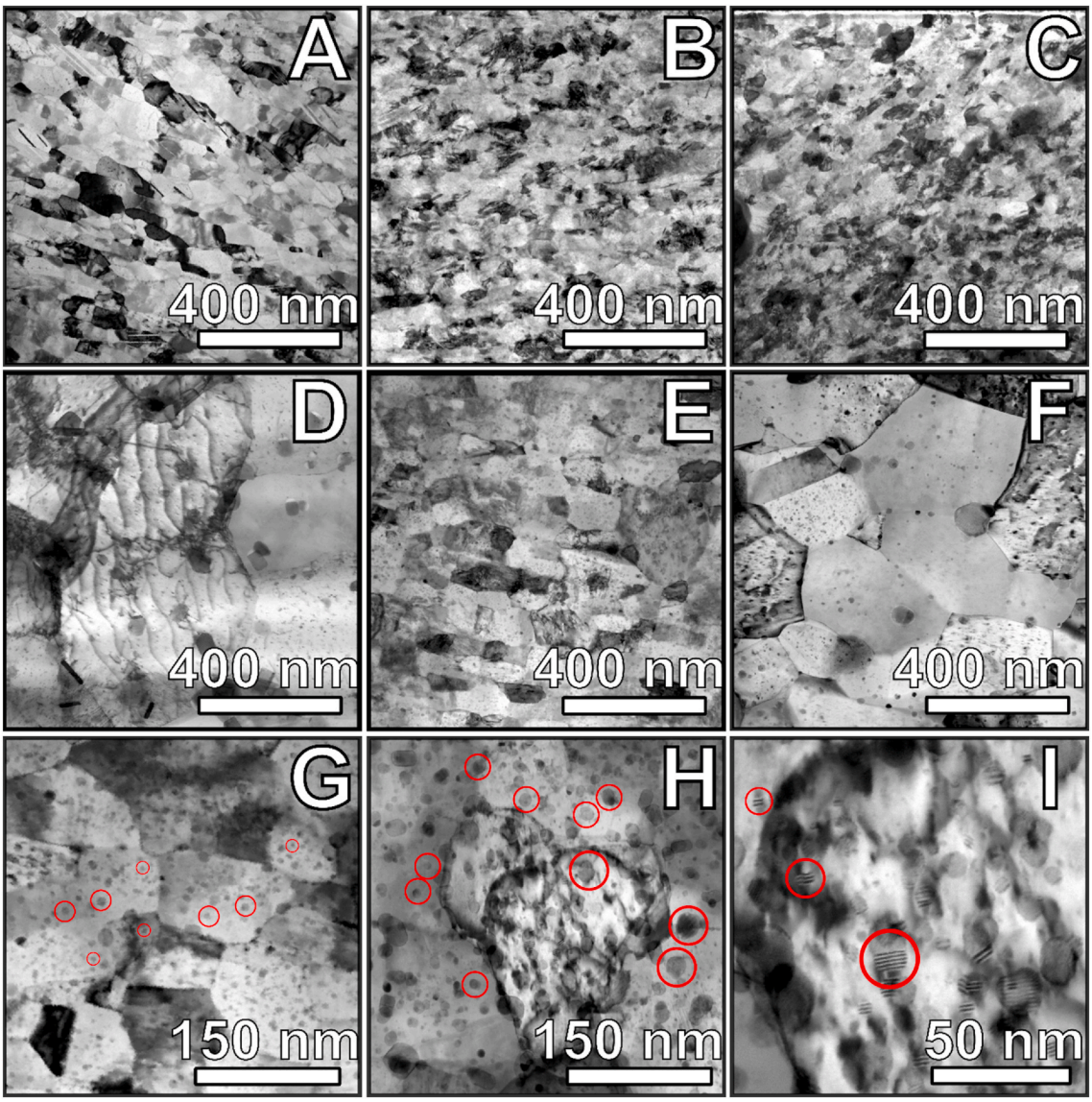

Fig. 3. STEM bright-field image after 1,000 h exposure to 600 °C for (a) Cu–1Ta, (b) Cu–3Ta, and (c) Cu–5Ta with a negligible change between 3 and 5Ta and only marginal coarsening in 1Ta. STEM bright-field image after 1,000 h exposure to 800 °C for (d) Cu–1Ta, (e) Cu–3Ta, and (f) Cu–5Ta confirming Cu–3Ta as the most thermally stable composition. STEM bright-field image of (G) Cu–3Ta after 1,000 h exposure to 800 °C with different size red rings corresponding to the different size Ta clusters they are encircling, (H) Cu–3Ta after 1-h exposure to 1050 °C (or 97.5% T_M). (I) Higher magnification STEM bright-field image of Cu–3Ta after 1-h exposure to 1050 °C highlighting the presence of Moiré fringes with the coarsened Ta particles. (For interpretation of the references to colour in this figure legend, the reader is referred to the Web version of this article.)

is much more favorable for long-term stabilization than all other compositions. Collectively, Fig. 2C-D shows that 3% is not only more thermally stable but additionally is stronger than both the 5% and 10% Ta alloys after exposure. This is an important observation, which also highlights the importance of studying much longer annealing times and/or high-temperature exposures (i.e., those greater than 100 h and 600 °C) since some kinetics processes may be very sluggish.

To provide correlations between the aging curves and microstructural evolution, STEM analysis was performed on samples of 1, 3, and 5% Ta content after annealing at 1,000 h at 800 °C, Fig. 3 D-F. STEM analysis of these samples reveals substantial differences in the microstructures that correlate with the aging curves at 800 °C. The 3% Ta microstructure retains a much finer grain size of ~ 96 ± 28 nm, while that of 5% has coarsened to 270 ± 94 nm and 1% coarsened to 383 ± 190 nm, see Fig. 4. To highlight the extreme stability of the 3% sample, it should be noted that the grain size, when exposed to 800 °C for ~1,000 h increased only 31 nm, i.e., from 65 nm after 1-h exposure to 96 nm after 1,000 h exposure (see Fig. 5 for comparative micrographs). To build off of this fact, it is important to remember that Cu–3Ta is an alloy composed of 97% Cu, which has maintained 80% of its peak yield strength (~900 MPa yield stress) after 1,000 h (41 days) of exposure to 80% T_M (800 °C). Thus, the Cu–3%Ta alloy has attained the yield strength of higher Ta-containing alloys with the stability of lower Ta-containing alloys, i.e., the alloy has attained a maximum between these two competing effects.

To further probe the Cu–3Ta alloys' thermal resiliency, we performed annealing studies at approximately 2.5% below Cu's absolute melting point (1357.6 K) for 1 h. The strength after exposure to this temperature resulted in estimated yield strength (from Vickers) of 650 MPa. For reference, NC-Cu with a grain size of 25–100 nm has similar room temperature yield strength [48]. However, these results are reported for Cu never having been exposed to any thermal treatment. Moreover, NC-Cu has a reported grain growth temperature of ~ 100 °C, upon which it undergoes extensive and rapid grain growth [12,13,

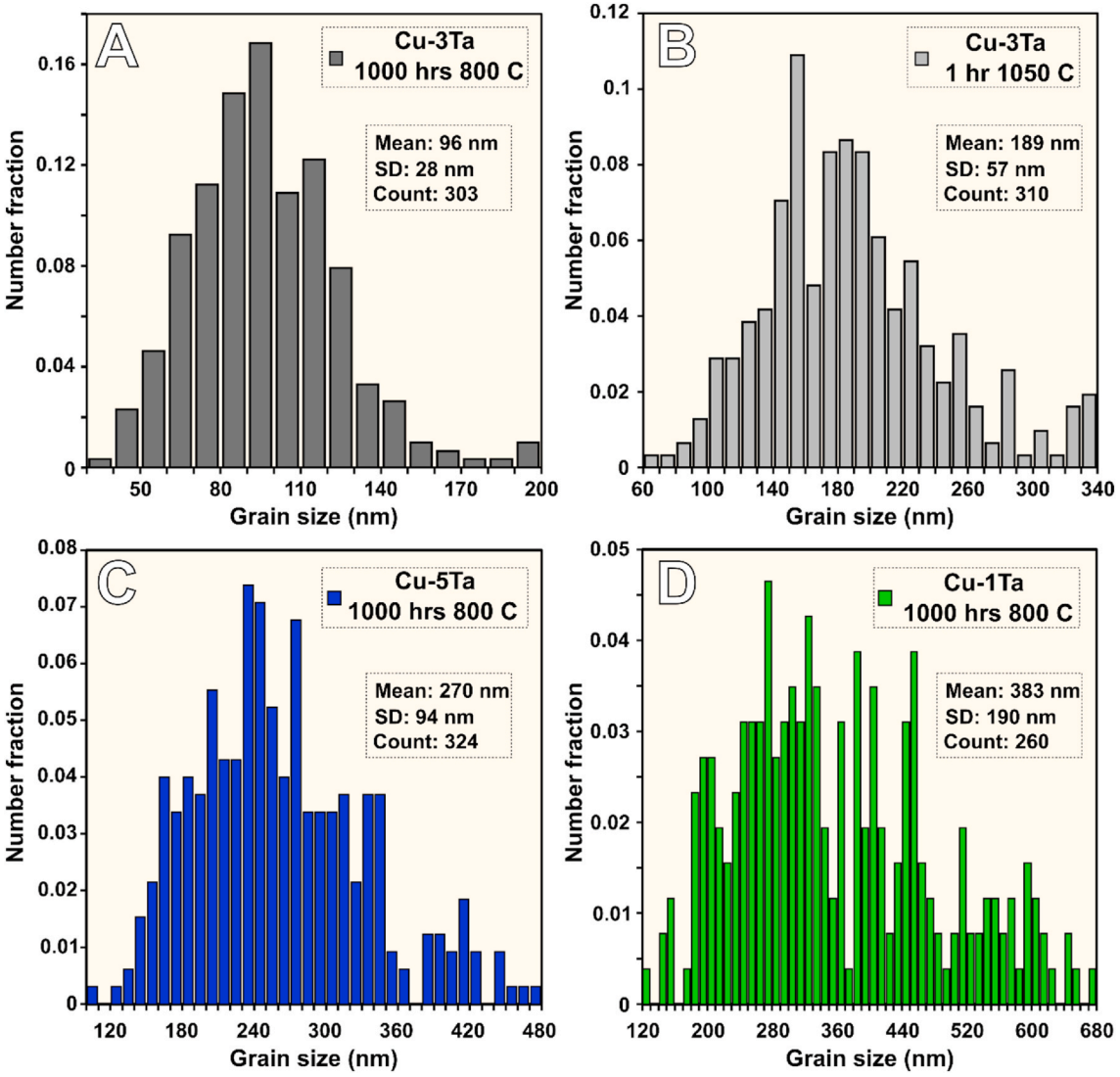

Fig. 4. Grain size distribution plots for (a) Cu–3Ta after 1,000 h exposure to 800 °C, (b) Cu–3Ta after 1-h exposure to 1050 °C (97.5% TM), (c) Cu–5Ta and (d) Cu–1Ta after 1,000 h exposure to 800 °C.

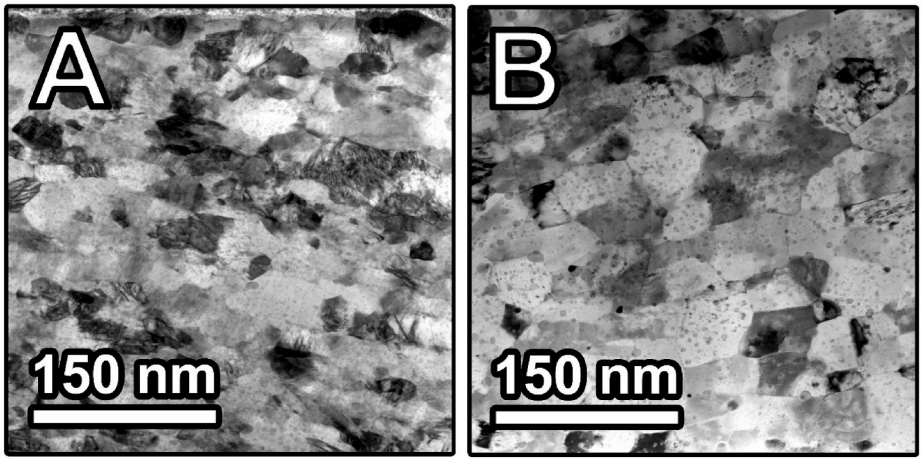

Fig. 5. STEM bright-field images of Cu–3Ta after exposure to 800 °C (80% T_M) for (a) 1 h and (b) 1,000 h highlighting the extreme thermal stability of the 3% sample with the grain size only increasing by 32 nm, i.e., from 65 nm to 97 nm.

49–53]. To put it in perspective, this is an order of magnitude lower than the annealing temperature NC-Cu-3Ta experienced. The grain size of the NC-Cu-3Ta, after annealing at 1050 °C was found to be 189 ± 57 nm. For an overall macroscopic view of the grain size and relevant microstructural features, see Fig. 6, which contains roughly 60 μm^2 of electron transparent area for each of the respective samples (1, 3, 5% Ta after 1, 000 h at 800 °C and 3% Ta after 1 h at 1050 °C). While the grain size has shown the most obvious sign of coarsening reported in the NC-Cu-3Ta alloy, the key microstructural feature to observe is the Ta particles. They too have coarsened to an average diameter of 6 nm moving them from the coherent to semi-coherent state, Fig. 3G–I. Accordingly, by lowering the number of coherent particles, the dominant stabilization mechanism in the Cu–3Ta alloy becomes less effective.

Note that in our previous work, refer to [37], we have characterized grain size and Ta-nanocluster size distributions, see Fig. 1 of [37]. As we discussed in Ref. [37], the smaller Ta-based nanoclusters possess an average diameter of 3.18 ± 0.86 nm. Further, the energy of the interface [55] between the nanocluster and the Cu matrix was used to quantify the type of coherency of these nanoclusters, and the range of the grain sizes which correspond to them. Characterizing the coherency at RT has indicated that this material has coherent, semicoherent, and incoherent nanoclusters (d < 3.9 nm, 3.9 to 15.6 nm, and >15.6 nm, respectively) [55]. Nevertheless, by comparing STEM images of the 1050 °C for 1 h versus the 800 °C for 1,000 h aged sample (Fig. 3 G and H), the discrepancy between the Ta-nanocluster size and number density and its effect on the grain size becomes abundantly clear. Hence, only by going to this incredibly high homologous temperature (97.5% T_M) is the short-circuit diffusion of Ta able to be accommodated within the Cu lattice. This accommodation allows minimal Ostwald ripening to coarsen the coherent Ta particle from a diameter of 3 nm to 6 nm on average. These coarsened Ta particles then lose some degree of their effectiveness (Zener) pinning force resulting in grain growth as seen in Fig. 3 G and H.

To further understand the annealing behavior of the NC-Cu-3Ta, analytical diffusion calculations were performed to conceptualize the change in magnitude the thermal energy has on the Cu–3Ta system and to highlight the extreme kinetics NC-Cu-3% Ta possesses. For example, at 800 °C for 1,000 h the mean free path of self-diffusion of Cu is 0.18 mm for lattice diffusion, while grain-boundary (GB) diffusion is 41.8 mm [56–58]. Note that for the lattice diffusion calculation, a value of 46.8 kcal/g-atom was used for the activation energy, Q, while 0.3 cm^2/s was used for the frequency factor, D_o [54]. For the grain boundary diffusion calculation, a value of 25 kcal/g-atom was used for the activation energy, Q, while 0.6 cm^2/s was used for the frequency factor, D_o [54]. For both calculations, the temperature, T, was 1073 K (800 °C), and the constant, R, was 8.314 J/K mol. Generally, due to the abundance of GBs in NC metals, the latter is the preferred diffusion mechanism controlling many aspects of their behavior [4]. Taking the measured grain size of 100 nm for the 3% Ta alloy, this equates to a Cu atom diffusing across the grain 1800 times using lattice diffusion and 400,000 times using GB diffusion. Despite the increased pressure associated with curvature-driven grain growth these grain size experiences at these temperatures, the boundaries remained fixed in place even though a tremendous amount of Cu diffusion had occurred at 800 °C during this extended time. Consequently, the authors have conceptualized the analogy of a chain-link fence, i.e., grain boundaries are able to flex but cannot migrate due to a large Zener pinning force associated with Ta-nanoclusters. In this analogy, the Ta-nanoclusters are the fence defining the GBs in which the Cu atoms can freely diffuse through without redefining the internal area of the grain/fenced area. This is reinforced by considering the grain size increased only 31 nm from 1 h to 1,000 h at 800 °C, which is equivalent to 3.1 nm of growth per 100 h assuming the steady-state rate stays constant. This overall stability is highlighted in Fig. 7A which shows the 3% alloy being ~3.5X more stable based on strength loss than its expected value, given the linear trend of the other compositions. This quantification was determined by

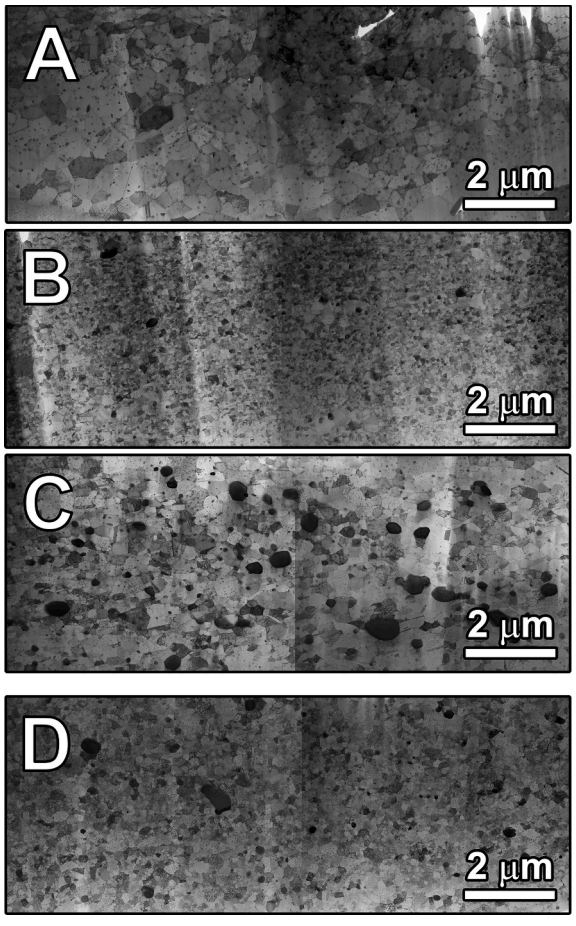

Fig. 6. STEM bright-field composite images showing roughly 60 μm^2 of electron transparent area: after 1,000 h of exposure to 800 °C for (a) Cu–1Ta, (b) Cu–3Ta, and (c) Cu–5Ta highlighting the minimal coarsening occurring in the 3Ta composition relative to the 1 and 5Ta. (d) Cu–3Ta after 1-h exposure to 1050 °C (97.5% TM) again speaking to the tremendous thermal stability of its microstructure.

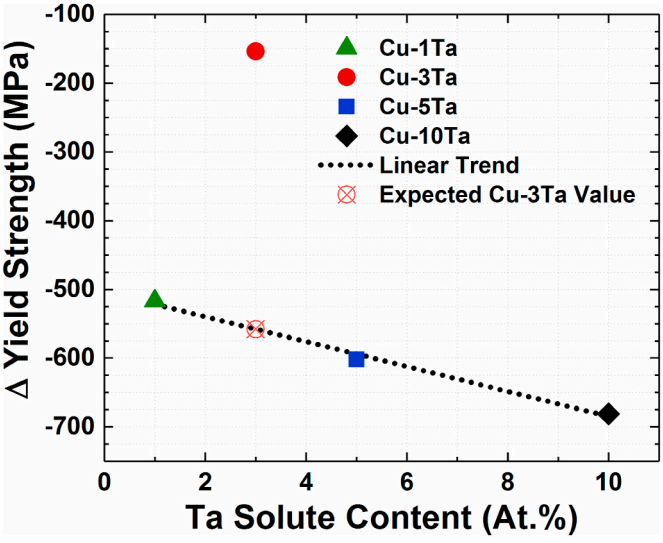

Fig. 7. Plot showing the substantial difference in the actual strength loss of Cu–3Ta compared to the expected value when linearly fitting the other compositions' strength loss both real and expected between their as-milled and after 1,000 h at 800 °C conditions.

plotting as a function of Ta content the difference in strength between the as-milled and after being exposed to 800 °C for 1000 h conditions for 1, 5, and 10% Ta alloys. The equation for this line ($Y = -18.132X - 503.14$) was then used to calculate the expected difference in strength values for alloy compositions ranging from 0 to 10. This was then overlaid with the actual measured values to yield Fig. 7. As can be seen, 3% provides a significant deviation in long-term stability which occurs over a relatively narrow composition. Hence, such demonstrations and tailoring of compositions are the logical steps if bulk NC metals are to be seriously considered viable candidates for advanced high-temperature applications, such as heat exchangers for nuclear applications and some turbine blade applications.

4. Conclusions

In summary, we address an important scientific question, i.e., if the exposure time is 1–2 orders of magnitude longer in real applications such as high-temperature turbine blades, is the perceived stability for NC alloys highlighted in literature after a few hundred hours or less, a relevant comparison to commercially available alloys successfully used for thousands of hours? Through addressing this, we also identified NC Cu-3 at.% Ta alloy, which shows only a 2% difference in its peak strength when exposed to 600 °C (65% T_M) for 1,000 h. Further validation is shown with the grain size coarsening by only 31 nm when exposed to 800 °C (~80% T_M) for approximately 1,000 h. In the most extreme case studied where the alloy is exposed to a homologous temperature 2.5% below its melting point, the dominant microstructural feature (Ta clusters) coarsened from 3 nm to 6 nm, yet a grain size of 189 ± 57 nm is still retained. This is in comparison to other compositions that underwent several hundreds of nanometers of grain growth and a dramatic reduction in their yield strength. These results clearly highlight the effect tailoring the Ta solute content has on stabilizing the growth of the clusters by kinetically limiting Orowan coarsening; thereby retaining the alloy's high strength after prolonged exposure to high homologous temperatures. In concluding, this manuscript highlights the critical importance of studying long exposure times since some of the traditional kinetic mechanisms may not be applicable, too slow, or non-traditional mechanisms may play a role; all of which are inaccessible during the shorter, traditional annealing studies reported in literature for NC alloys.

Data availability

The raw/processed data required to reproduce these findings cannot be shared at this time due to legal or ethical reasons.

CRediT authorship contribution statement

B.C. Hornbuckle: Conceptualization, Methodology, Investigation, Formal analysis, Writing – original draft, Writing – review & editing. **K. Solanki:** Writing – original draft, Writing – review & editing. **K.A. Darling:** Visualization, Supervision, Writing – original draft, Writing – review & editing.

Declaration of competing interest

The authors declare that they have no known competing financial interests or personal relationships that could have appeared to influence the work reported in this paper.

Acknowledgment

K.S is supported by Army Research Laboratory award number W911NF-15-2-0038 and the National Science Foundation award number 1663287.

Appendix

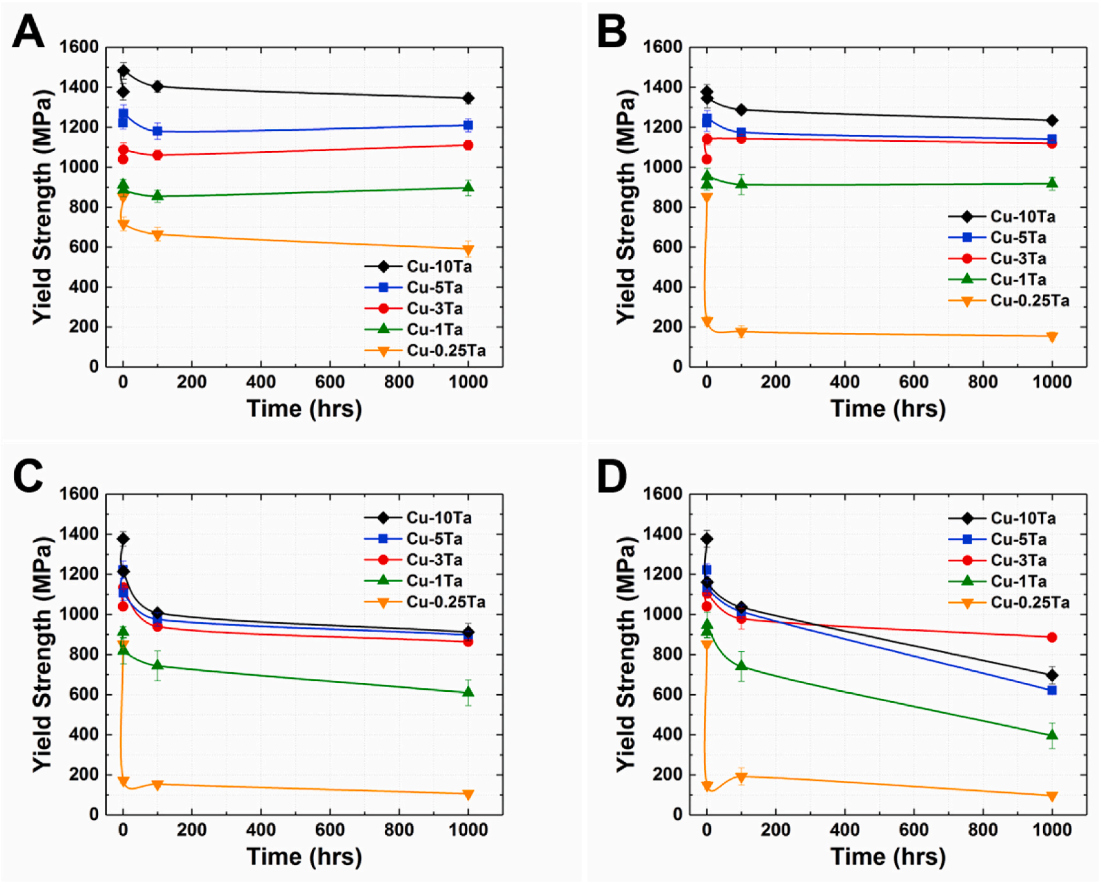

Fig. A1. Yield strength for various compositions plotted as a function of time at annealing temperatures of (A) 400 °C, (B) 600 °C, (C) 700 °C, and (D) 800 °C.

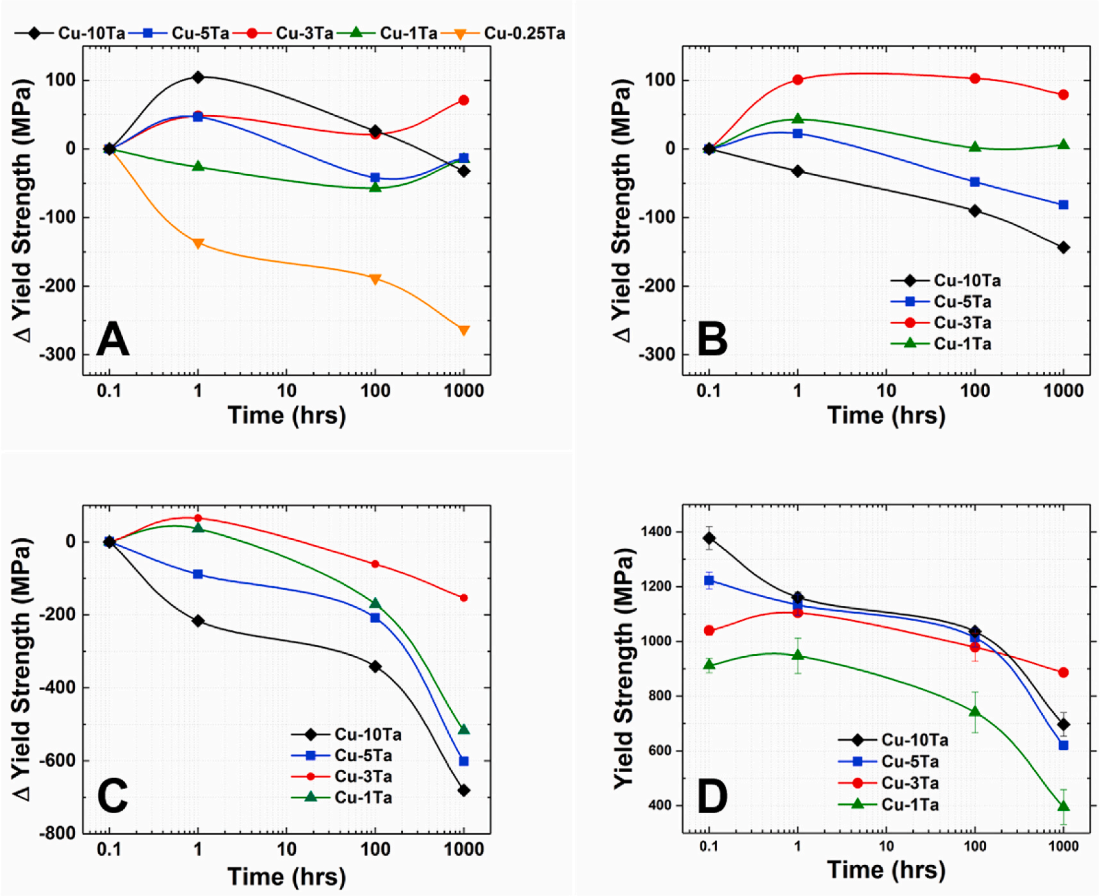

Fig. A2. Change in yield strength relative to each compositions' as-milled yield strength after 1,000 h of isothermal annealing at (a) 400 °C (50% T_M), (b) 600 °C (65% T_M), and (c) 800 °C (80% T_M) respectively. (d) Yield strength curves for the various compositions aged at 800 °C out to 1,000 h (Duplicate figure of Fig. 2 but with the x-axis plotted on a logarithmic versus a linear scale.).

References

[1] G.S. Was, Fundamentals of Radiation Materials Science: Metals and Alloys, second ed., Springer-Verlag, New York, 2017. https://www.springer.com/gp/book/9781493934362.

[2] T. Ghidini, Materials for space exploration and settlement, Nat. Mater. 17 (2018) 846–850, https://doi.org/10.1038/s41563-018-0184-4.

[3] A.P. Mouritz, Introduction to Aerospace Materials, Elsevier, 2012.

[4] M.A. Meyers, A. Mishra, D.J. Benson, Mechanical properties of nanocrystalline materials, Prog. Mater. Sci. 51 (2006) 427–556, https://doi.org/10.1016/j.pmatsci.2005.08.003.

[5] H. Gleiter, Nanostructured materials: basic concepts and microstructure, Acta Mater. 48 (2000) 1–29, https://doi.org/10.1016/S1359-6454(99)00285-2.

[6] K. Lu, Stabilizing nanostructures in metals using grain and twin boundary architectures, Nat. Rev. Mater. 1 (2016), natrevmats201619, https://doi.org/10.1038/natrevmats.2016.19.

[7] C.C. Koch, Structural nanocrystalline materials: an overview, J. Mater. Sci. 42 (2007) 1403–1414.

[8] H.A.P. Ii, B.L. Boyce, A review of fatigue behavior in nanocrystalline metals, Exp. Mech. 50 (2010) 5–23, https://doi.org/10.1007/s11340-009-9301-2.

[9] K.S. Kumar, H. Van Swygenhoven, S. Suresh, Mechanical behavior of nanocrystalline metals and alloys, Acta Mater. 51 (2003) 5743–5774, https://doi.org/10.1016/j.actamat.2003.08.032.

[10] A.H. Chokshi, Unusual stress and grain size dependence for creep in nanocrystalline materials, Scripta Mater. 61 (2009) 96–99, https://doi.org/10.1016/j.scriptamat.2009.03.009.

[11] T.J. Rupert, D.S. Gianola, Y. Gan, K.J. Hemker, Experimental observations of stress-driven grain boundary migration, Science 326 (2009) 1686–1690, https://doi.org/10.1126/science.1178226.

[12] L. Lu, N.R. Tao, L.B. Wang, B.Z. Ding, K. Lu, Grain growth and strain release in nanocrystalline copper, J. Appl. Phys. 89 (2001) 6408–6414, https://doi.org/10.1063/1.1367401.

[13] Y. Hunag, A. Menovsky, F. De Boer, Calorimetric analysis of the grain growth in nanocrystalline copper samples, Nanostruct. Mater. 2 (1993) 587–595, https://doi.org/10.1016/0965-9773(93)90032-7.

[14] F. Abdeljawad, P. Lu, N. Argibay, B.G. Clark, B.L. Boyce, S.M. Foiles, Grain boundary segregation in immiscible nanocrystalline alloys, Acta Mater. 126 (2017) 528–539, https://doi.org/10.1016/j.actamat.2016.12.036.

[15] M. Akbarpour, H. Kim, Microstructure, grain growth, and hardness during annealing of nanocrystalline Cu powders synthesized via high energy mechanical milling, Mater. Des. 83 (2015) 644–650.

[16] X.H. An, S.D. Wu, Z.G. Wang, Z.F. Zhang, Enhanced cyclic deformation responses of ultrafine-grained Cu and nanocrystalline Cu–Al alloys, Acta Mater. 74 (2014) 200–214, https://doi.org/10.1016/j.actamat.2014.04.053.

[17] M. Ames, J. Markmann, R. Karos, A. Michels, A. Tschöpe, R. Birringer, Unraveling the nature of room temperature grain growth in nanocrystalline materials, Acta Mater. 56 (2008) 4255–4266.

[18] S. Simoes, R. Calinas, M. Vieira, M. Vieira, P.J. Ferreira, In situ TEM study of grain growth in nanocrystalline copper thin films, Nanotechnology 21 (2010) 145701.

[19] O. Yevtushenko, H. Natter, R. Hempelmann, Grain-growth kinetics of nanostructured gold, Thin Solid Films 515 (2006) 353–356.

[20] G. Sharma, J. Varshney, A. Bidaye, J. Chakravartty, Grain growth characteristics and its effect on deformation behavior in nanocrystalline Ni, Mater. Sci. Eng. A. 539 (2012) 324–329.

[21] G.D. Hibbard, V. Radmilovic, K.T. Aust, U. Erb, Grain boundary migration during abnormal grain growth in nanocrystalline Ni, Mater. Sci. Eng. A. 494 (2008) 232–238, https://doi.org/10.1016/j.msea.2008.04.054.

[22] H. Natter, M. Schmelzer, R. Hempelmann, Nanocrystalline nickel and nickel-copper alloys: synthesis, characterization, and thermal stability, J. Mater. Res. 13 (1998) 1186–1197, https://doi.org/10.1557/JMR.1998.0169.

[23] H.A. Padilla, B.L. Boyce, A review of fatigue behavior in nanocrystalline metals, Exp. Mech. 50 (2010) 5–23, https://doi.org/10.1007/s11340-009-9301-2.

[24] M.D. Sangid, G.J. Pataky, H. Sehitoglu, R.G. Rateick, T. Niendorf, H.J. Maier, Superior fatigue crack growth resistance, irreversibility, and fatigue crack growth–microstructure relationship of nanocrystalline alloys, Acta Mater. 59 (2011) 7340–7355, https://doi.org/10.1016/j.actamat.2011.07.058.

[25] A. Witney, P. Sanders, J. Weertman, J. Eastman, Fatigue of nanocrystalline copper, Scripta Metall. Mater. 33 (1995).

[26] C.J. Shute, B. Myers, S. Xie, T. Barbee Jr., A. Hodge, J. Weertman, Microstructural stability during cyclic loading of multilayer copper/copper samples with nanoscale twinning, Scripta Mater. 60 (2009) 1073–1077.

[27] T.R. Malow, C.C. Koch, Grain growth in nanocrystalline iron prepared by mechanical attrition, Acta Mater. 45 (1997) 2177–2186, https://doi.org/10.1016/S1359-6454(96)00300-X.
[28] D.S. Gianola, S. Van Petegem, M. Legros, S. Brandstetter, H. Van Swygenhoven, K. J. Hemker, Stress-assisted discontinuous grain growth and its effect on the deformation behavior of nanocrystalline aluminum thin films, Acta Mater. 54 (2006) 2253–2263, https://doi.org/10.1016/j.actamat.2006.01.023.
[29] A.H. Chokshi, Unusual stress and grain size dependence for creep in nanocrystalline materials, Scripta Mater. 61 (2009) 96–99, https://doi.org/10.1016/j.scriptamat.2009.03.009.
[30] F.A. Mohamed, Y. Li, Creep and superplasticity in nanocrystalline materials: current understanding and future prospects, Mater. Sci. Eng. A. 298 (2001) 1–15, https://doi.org/10.1016/S0928-4931(00)00190-9.
[31] B. Cai, Q.P. Kong, L. Lu, K. Lu, Low temperature creep of nanocrystalline pure copper, Mater. Sci. Eng. A. 286 (2000) 188–192, https://doi.org/10.1016/S0921-5093(00)00633-X.
[32] W. Yin, S. Whang, R. Mirshams, C. Xiao, Creep behavior of nanocrystalline nickel at 290 and 373 K, Mater. Sci. Eng. A. 301 (2001) 18–22.
[33] J. Li, J.Y. Zhang, G. Liu, J. Sun, New insight into the stable grain size of nanotwinned Ni in steady-state creep: effect of the ratio of effective-to-internal stress, Int. J. Plast. 85 (2016) 172–189, https://doi.org/10.1016/j.ijplas.2016.07.009.
[34] R.K. Koju, K.A. Darling, K.N. Solanki, Y. Mishin, Atomistic modeling of capillary-driven grain boundary motion in Cu-Ta alloys, Acta Mater. 148 (2018) 311–319, https://doi.org/10.1016/j.actamat.2018.01.027.
[35] K.A. Darling, M. Rajagopalan, M. Komarasamy, M.A. Bhatia, B.C. Hornbuckle, R. S. Mishra, K.N. Solanki, Extreme creep resistance in a microstructurally stable nanocrystalline alloy, Nature 537 (2016) 378–381, https://doi.org/10.1038/nature19313.
[36] C. Kale, S. Srinivasan, B.C. Hornbuckle, R.K. Koju, K. Darling, Y. Mishin, K. N. Solanki, An experimental and modeling investigation of tensile creep resistance of a stable nanocrystalline alloy, Acta Mater. 199 (2020) 141–154, https://doi.org/10.1016/j.actamat.2020.08.020.
[37] M. Rajagopalan, K. Darling, S. Turnage, R. Koju, B. Hornbuckle, Y. Mishin, K. Solanki, Microstructural evolution in a nanocrystalline Cu-Ta alloy: a combined in-situ TEM and atomistic study, Mater. Des. 113 (2017) 178–185.
[38] M.A. Meyers, K.K. chawla, Mechanical Behavior Materials, second ed., Cambridge University Press, United Kingdom, 2008. http://www.cambridge.org/us/academic/subjects/engineering/materials-science/mechanical-behavior-materials-2nd-edition. (Accessed 24 May 2017).
[39] K.A. Darling, A.J. Roberts, Y. Mishin, S.N. Mathaudhu, L.J. Kecskes, Grain size stabilization of nanocrystalline copper at high temperatures by alloying with tantalum, J. Alloys Compd. 573 (2013) 142–150, https://doi.org/10.1016/j.jallcom.2013.03.177.
[40] K.A. Darling, M.A. Tschopp, R.K. Guduru, W.H. Yin, Q. Wei, L.J. Kecskes, Microstructure and mechanical properties of bulk nanostructured Cu–Ta alloys consolidated by equal channel angular extrusion, Acta Mater. 76 (2014) 168–185, https://doi.org/10.1016/j.actamat.2014.04.074.
[41] B.C. Hornbuckle, T. Rojhirunsakool, M. Rajagopalan, T. Alam, G.P.P. Pun, R. Banerjee, K.N. Solanki, Y. Mishin, L.J. Kecskes, K.A. Darling, Effect of Ta solute concentration on the microstructural evolution in immiscible Cu-Ta alloys, JOM 67 (2015) 2802–2809, https://doi.org/10.1007/s11837-015-1643-x.
[42] M. Bhatia, M. Rajagopalan, K. Darling, M. Tschopp, K. Solanki, The role of Ta on twinnability in nanocrystalline Cu–Ta alloys, Mater. Res. Lett. 5 (2017) 48–54.
[43] M. Rajagopalan, K.A. Darling, C. Kale, S.A. Turnage, R.K. Koju, B.C. Hornbuckle, Y. Mishin, K.N. Solanki, Nanotechnology enabled design of a structural material with extreme strength as well as thermal and electrical properties, Mater. Today 31 (2019) 10–20, https://doi.org/10.1016/j.mattod.2019.09.024.
[44] T. Frolov, K.A. Darling, L.J. Kecskes, Y. Mishin, Stabilization and strengthening of nanocrystalline copper by alloying with tantalum, Acta Mater. 60 (2012) 2158–2168, https://doi.org/10.1016/j.actamat.2012.01.011.
[45] K.A. Darling, C. Kale, S. Turnage, B.C. Hornbuckle, T.L. Luckenbaugh, S. Grendahl, K.N. Solanki, Nanocrystalline material with anomalous modulus of resilience and springback effect, Scripta Mater. 141 (2017) 36–40, https://doi.org/10.1016/j.scriptamat.2017.07.012.
[46] B.C. Hornbuckle, C. Kale, S. Srinivasan, T.L. Luckenbaugh, K.N. Solanki, K. A. Darling, Revealing cryogenic mechanical behavior and mechanisms in a microstructurally-stable, immiscible nanocrystalline alloy, Scripta Mater. 160 (2019) 33–38, https://doi.org/10.1016/j.scriptamat.2018.09.035.
[47] S.A. Turnage, M. Rajagopalan, K.A. Darling, P. Garg, C. Kale, B.G. Bazehhour, I. Adlakha, B.C. Hornbuckle, C.L. Williams, P. Peralta, K.N. Solanki, Anomalous mechanical behavior of nanocrystalline binary alloys under extreme conditions, Nat. Commun. 9 (2018) 2699, https://doi.org/10.1038/s41467-018-05027-5.
[48] M.A. Tschopp, H.A. Murdoch, L.J. Kecskes, K.A. Darling, "Bulk" nanocrystalline metals: review of the current state of the art and future opportunities for copper and copper alloys, JOM 66 (2014) 1000–1019, https://doi.org/10.1007/s11837-014-0978-z.
[49] Y. Zhang, G.J. Tucker, J.R. Trelewicz, Stress-assisted grain growth in nanocrystalline metals: grain boundary mediated mechanisms and stabilization through alloying, Acta Mater. 131 (2017) 39–47, https://doi.org/10.1016/j.actamat.2017.03.060.
[50] H. Jiang, Y.T. Zhu, D.P. Butt, I.V. Alexandrov, T.C. Lowe, Microstructural evolution, microhardness and thermal stability of HPT-processed Cu, Mater. Sci. Eng. A. 290 (2000) 128–138, https://doi.org/10.1016/S0921-5093(00)00919-9.
[51] L. Lu, M.L. Sui, K. Lu, Cold rolling of bulk nanocrystalline copper, Acta Mater. 49 (2001) 4127–4134, https://doi.org/10.1016/S1359-6454(01)00248-8.
[52] L. Lu, L.B. Wang, B.Z. Ding, K. Lu, Comparison of the thermal stability between electro-deposited and cold-rolled nanocrystalline copper samples, Mater. Sci. Eng. A. 286 (2000) 125–129, https://doi.org/10.1016/S0921-5093(00)00712-7.
[53] J. Eckert, J.C. Holzer, C.E. Krill, W.L. Johnson, Structural and thermodynamic properties of nanocrystalline fcc metals prepared by mechanical attrition, J. Mater. Res. 7 (1992) 1751–1761, https://doi.org/10.1557/JMR.1992.1751.
[54] W. Callister, D. Rethwisch, Materials Science and Engineering: an Introduction, tenth ed., Wiley, 2018. https://www.wiley.com/en-us/Materials+Science+and+Engineering%3A+An+Introduction%2C+10th+Edition-p-9781119405498.
[55] J.D. Eshelby, The determination of the elastic field of an ellipsoidal inclusion, and related problems, Proc. R. Soc. Lond. Math. Phys. Eng. Sci. 241 (1957) 376–396, https://doi.org/10.1098/rspa.1957.0133.
[56] A. Kuper, H. Letaw, L. Slifkin, E. Sonder, C.T. Tomizuka, Self-diffusion in copper, Phys. Rev. 96 (1954) 1224–1225, https://doi.org/10.1103/PhysRev.96.1224.
[57] D.B. Butrymowicz, J.R. Manning, M.E. Read, Diffusion in copper and copper alloys. Part I. Volume and surface self-diffusion in copper, J. Phys. Chem. Ref. Data 2 (1973) 643–656, https://doi.org/10.1063/1.3253129.
[58] J. Askill, Tracer Diffusion Data for Metals, Alloys, and Simple Oxides, Springer Science & Business Media, 2012.